heritage

MDPI

Article

Characterization of the Stone Masonries and Evaluation of the Environmental Impact in Panamá Viejo: A Contribution for the Conservation of the Monumental Complex

Chiara Ciantelli [1,*], Silvia I. Arroyo Duarte [2,3], Carmela Vaccaro [4] and Alessandra Bonazza [5]

[1] ENEA Brasimone Research Centre, Camugnano, 40032 Bologna, Italy
[2] Art Department, Facultad de Arquitectura, Universidad de Panamá, (Campus Universitario Octavio Méndez Pereira), Ciudad Universitaria Estafeta Universitaria, Apartado 3366, Panama; silvia.arroyo@up.ac.pa
[3] Sistema Nacional de Investigación (SNI), Panama 01001, Panama
[4] Department of Environmental and Prevention Science, University of Ferrara, C.So Ercole I d'Este 32, 44121 Ferrara, Italy; vcr@unife.it
[5] Institute of Atmospheric Sciences and Climate, National Research Council of Italy, Via Gobetti 101, 40129 Bologna, Italy; a.bonazza@isac.cnr.it
* Correspondence: chiara1309@gmail.com or chiara.ciantelli@enea.it

Abstract: A fundamental step in the best preservation of heritage materials is investigating their chemical and physical characteristics, and understanding how they interact with the surrounding environment. For this reason, the stone masonry of the monumental UNESCO site of Panamá Viejo was subjected to a thorough study to characterize the materials and evaluate their state of conservation. Additionally, potential outcrops were explored in order to identify sites for the supply of raw materials. The methodological approach encompassed mineralogical-petrographic investigations using stereomicroscopy, polarized light microscopy (PLM), X-ray powder diffraction (XRPD), scanning electron microscopy and energy dispersive X-ray spectrometry (ESEM-EDS) and X-ray fluorescence (XRF). The results revealed that the masonries primarily consists of polygenic breccia, basaltic andesite, rhyodacite, tuffite, and rhyolite. In addition, at the potential quarries, breccia and basaltic andesite were identified. The porous structure was studied using mercury intrusion porosimetry (MIP). Possible issues due to salt dissolution/crystallization cycles were considered. Consequently, ion chromatography (IC) was conducted on samples exhibiting alteration patinas to study the presence of soluble salts. In assessing the state of conservation, prevalent forms of deterioration included biological colonization, detachments, material loss, potential salt weathering, and chromatic alteration. In conclusion, the outcomes of this work provide a valuable resource for the current and future preservation of this site.

Keywords: building material characterization; environmental impact; deterioration process; weathering; Panamanian heritage; historical monumental complex

check for updates

Citation: Ciantelli, C.; Arroyo Duarte, S.I.; Vaccaro, C.; Bonazza, A. Characterization of the Stone Masonries and Evaluation of the Environmental Impact in Panamá Viejo: A Contribution for the Conservation of the Monumental Complex. *Heritage* **2023**, *6*, 6526–6546. https://doi.org/10.3390/heritage6100341

Academic Editors: Mauro Francesco La Russa, Patricia Sanmartín and Nick Schiavon

Received: 26 July 2023
Revised: 2 September 2023
Accepted: 12 September 2023
Published: 25 September 2023

Copyright: © 2023 by the authors. Licensee MDPI, Basel, Switzerland. This article is an open access article distributed under the terms and conditions of the Creative Commons Attribution (CC BY) license (https://creativecommons.org/licenses/by/4.0/).

1. Introduction

Nowadays, the Republic of Panama is mostly known for its renowned Canal, an immense engineering work of significant global trade importance. Situated in the narrowest part of the isthmus of the American continent, Panama has held its role as a strategic crossroad for commercial routes since the 16th century. During this period, it has served as a crucial link between the "New World" and the "Old World".

It hosted the first Spanish settlement on the Pacific Coast, presently referred to as the "Monumental Complex of Panamá Viejo", which is nationally used by law, while internationally, it is known as the "Archaeological Site of Panamá Viejo". Founded more than 500 years ago, precisely on the 15th of August 1519, and due to its exceptional significance, the site was included as an extension of the Historic District of Panama on the World Heritage List in 2003 [1,2].

A few years before, a private, autonomous, non-profit organization of public interest was established: the Patronato of Panamá Viejo. Its mission aims at managing, preserving, and promoting the site [3]. In the pursuit of supporting the conservation and valorization of this unique heritage site, a collaboration started in 2014 among the Patronato, the Institute of Atmospheric Sciences and Climate of the Italian National Research Council (ISAC-CNR), and the Department of Earth Sciences of the University of Ferrara. The central focus of this work was investigating the effects of climate and pollution on the construction materials [4].

In 2014, a sampling campaign was performed to gather representative specimens of the stone masonry buildings and identify potential quarries for the supply of raw materials. Additional information regarding the sampling approach and the analytical techniques are reported in the "Section 2. Materials and Methods" paragraph. Therefore, this study represents an innovative field of research in this region. It offers an exploration on the lithologies utilized as construction materials at the Panamá Viejo site. Moreover, it assesses their state of preservation, considering the interaction between the materials and the environment.

1.1. Historical Background and Site Location

The Monumental Complex of Panamá Viejo, which was originally 60 hectares in size, now encompasses 28 hectares, i.e., when considering the protected area. It extends along the Pacific Coast, situated between the río Algarrobo on the west side and the río Abajo (originally known as the río Gallinero) on the east side, as depicted in Figure 1.

Figure 1. Google Earth-modified image of the Monumental Complex of Panamá Viejo, surrounded by the urban context of Panama City. The dashed line indicates the current path of the Avenida Cincuentenario.

Before becoming the first European outpost on the American Pacific, this area hosted a fishing village belonging to the indigenous Cueva population, with its settlement dating back to approximately 500 AD.

Following the foundation of Panamá Viejo in the 16th century by Pedrarias Dávila, the significance of this site grew over the course of a century and a half. The town was structured with a main square, called Plaza Mayor, located near the sea. The urban layout was characterized by an almost rectilinear grid, an example of early European colonial urbanism [5–7].

During the 17th century, the site faced two traumatic events: in 1621, the town was struck by an earthquake and, in 1671, a devasting fire broke out at the site. Subsequent to the latter catastrophe, the settlement was relocated to the current Historic District of Panama, also known as Casco Antiguo. This is situated close to the Ancón Hill, with a superior and

more strategic position. The original town was destructed and abandoned, with many of its remains used as a quarry for constructing the "new" Casco Antiguo [5,8–11].

Today, the site hosts the remnants of buildings constructed during the period between the late 16th century and the 17th century. The majority of these are stone masonry structures belonging to monastic complexes, public and private constructions, each serving particular and/or strategic functions. The custom of exclusively using natural stone for government buildings, churches, convents, and the finest houses began in the late 16th century. However, according to the literature, there were three distinct construction styles: entirely wooden structures, entirely stonework buildings, and a mixed type featuring stone on the lower floor and wood on the upper floor [12]. Only the stonework type has survived to the present day, which was constructed with rocks and mortars. Consequently, the focus of this study is on the stone of this typology of masonry, while the mortar elements were investigated in a previous work [13].

Finally, it is important to mention that it is highly likely that the stone used in the construction was sourced directly from the surrounding area, considering the proximity of quarries [14]. This is documented in a letter dated 1608, from Bartolomé Morquecho to the King, stating: "there is stone in the suburbs of this city, it is very good and at little cost" [15]. The transport of stone from Panama to Peru during the 17th century has also been examined, revealing the abundant availability of the material [12]. For this reason, three outcrops, i.e., potential quarries for the materials used in the stone masonry, were identified and studied.

1.2. Environmental Context

Considering the environmental setting, the site is situated directly facing the ocean, which has led to progressive coastal erosion over the past five centuries [16–18]. Presently, the ruins of Panamá Viejo stand approximately 100 m away from the sea [19]. The nearest complex to the shoreline on the western side, Casas Reales, has experienced erosion from tides (Figure 2). In 2008, the consolidation of Casas Reales was performed using traditional materials and construction methods. The walls facing the sea were consolidated and a buttress was built to replace and counter the material loss, preventing the collapse of the wall. Reintegration, waterproofing, and injections were also executed. Additionally, the area surrounding the monument's ruins was backfilled with soil to mitigate the impact of the sea [20]. It should be noted that the Pacific coast experiences a daily average tidal range of 1.5 m, which occurs twice daily and exhibits periodic peak values of 6.7 m [17].

Figure 2. Walls of the Casas Reales Complex. The bottom part still shows the erosion due to the tides "carving" effect.

According to the "thermal zones of the Earth", a climate classification developed by Köppen–Geiger and validated for the latter half of the 20th century by Kottek et al. [21],

the Panamanian region falls under the A category, indicating an equatorial climate zone characterized by two distinct seasons: the dry and rainy season. The latter is the longer of the two, approximately covering the period from April until November/December. For that reason, annual precipitation amount is notably high, with values reaching 2300 mm along the Pacific littoral. Regarding temperature, minimal fluctuations occur throughout the year, maintaining an annual mean of 27 °C. The monthly average relative humidity, recorded at Tocumen (near Panama City), from 1979 to 2008, was approximately between 70% and 85% [22]. Given these thermo-hygrometric conditions, stone masonry can potentially undergo salt weathering, which could lead to disintegration and detachments due to internal material stresses [23].

Furthermore, in Panama, rainfall tends to be intense and of a short duration. This, coupled with the growth of urbanization, has caused the increase in surface runoff. Such runoff has the potential to carry dissolved contaminants, including salts and pollutants, representing a possible further source of danger for the materials [24]. In addition, the high intensity of rainfall can trigger related effects on exposed monuments, such as heightening mechanical erosion and chemical deterioration, due to water permeating the structures [25]. Moreover, the changing of climate can trigger deterioration phenomena in a different way in comparison with nowadays. Phenomena closely linked to precipitation amounts have been previously examined, revealing that the Panamá Viejo area could experience an increment of surface recession on carbonate rocks and the biomass accumulation on hard acid stones could be fostered in the near and distant future [22].

Lastly, the anthropic context should be considered. Panamá Viejo is totally embedded in the urban context of Panama City. Between 1950 and 2013, the monumental site was crossed by one of the city's major traffic routes, Avenida Cincuentenario, connecting significant locations such as the airport. Currently, this street runs along the northern part of the archaeological site, providing better protection for the monuments against the impact of pollution.

1.3. Geological and Geomorphological Setting

The complex region formation is due to multifarious interactions among five plates: two continental, the North and South American plates, and three oceanic shelfs called Caribbean, Cocos, and Nazca. The latter one is still subducting beneath the Panamanian portion of the Caribbean Plate [26].

As it is justifiable and in line with to the statement of Cunningham et al. [27], nearly 70 percent of the isthmus consists of volcanic rocks. Observing the surroundings of Panamá Viejo, the formations present are Panamá, marine facies (tuffaceous sandstone and siltstones, algal and foraminifera limestones) and volcanic facies (agglomerates, generally andesitic in fine-grained tuffs, and streamed deposited conglomerates). Moreover, there is La Boca formation (with siltstones, sandstone, tuff, and limestones). Lastly, there are alluvium or fill sediments, along with basalts and andesites.

Focusing specifically on the Panamá Viejo site, a thesis research performed specific analysis on the geology of the archaeological site. It realized a characterization of the superficial soil in order to establish a geological pattern of the area where the colonial structures are erected [28]. The study showed the presence of a volcanic eruption on the coast near the Casas Reales complex. Specifically, the rocks, showing an aphanitic texture, are mainly andesite, displaying surface oxidation. In addition, andesitic agglomerates were detected. Finally, pyroclastic outcrops were also identified near the complex of the Torre de la Catedral. In Panama, rock outcrops are present throughout almost the entire coastal area. They can be seen by the naked eye at the archaeological site, in areas close to the cathedral, the convent of Santo Domingo, and even in Casas Reales. In both cases of Casas Reales and the Torre de la Catedral, these outcrops were used also as foundations, offering stable ground [14].

2. Materials and Methods

Among the monuments of the complex, eight structures were carefully chosen for investigation. The selection was based on their significance and with the aim of providing a comprehensive representation of the entire site, in accordance with the patronage [4,13]. For evaluating different environmental conditions, structures situated in different positions were considered, such as those near the sea, those farther away, those adjacent to roads, and those that are not. The selected monuments are outlined below, ordered from the site's eastern side to its western side. Their respective locations are illustrated in Figure 3.

Figure 3. (**a**) Google Earth-modified image of the monumental complex of Panamá Viejo and list of the monuments and outcrops sampled with their locations. (**b**–**f**) Monuments sampled and examples of specimens collected: (**b**) Fortín de la Natividad; (**c**) Convento de San Francisco, (**d**) Convento de las Monjas de la Concepción; (**e**) Torre de la Catedral; (**f**) Casa Terrin; (**g**) outcrop sampled near Casas Reales Complex; (**h**) outcrop showing traces of possible quarrying activities near the Convento de Santo Domingo.

1. Fortín de la Natividad: Constructed during the 17th century on the eastern side of the site. Currently located near the new Vía Cincuentenario and in front of a gas station;
2. Convento de San Francisco: The construction began in 1603, situated in the eastern part of the archaeological site, adjacent to the new Vía Cincuentenario. It was one of the largest convents in Panamá Viejo, initially occupying around 5000 m^2, which is now reduced to 3000 m^2;
3. Hospital de San Juan de Dios: Initially known as the "Saint Sebastian Hospital", built two years after the foundation of the town. Renamed San Juan de Dios from 1620 onwards, it was named after the order that took over the hospital. The original area of the convent was 2500 m^2, and is now reduced to 1500 m^2. It consisted of a

large stonewall structure incorporating a church, cloisters, rooms, patios, and the military hospital;

4. Convento de las Monjas de la Concepción: Occupies an area of 1500 m^2 on the western side of the town. The church was constructed a century later than the town's foundation. In the 20th century, its ruins were damaged by the construction of a street perpendicular to Vía Cincuentenario, dividing the complex and the church in half;
5. Convento de la Compañía de Jesús: Established in 1578 and located near the Plaza Mayor. Originally made of wood, but from the beginning of the 17th century, the convent was converted into stone masonry. The remaining structures include the church and the primary cloisters, dating back to after the 1621 earthquake;
6. Casa Terrín: Overlooking the Plaza Mayor, this structure was constructed around 1600 by Francisco Terrín, one of the most powerful inhabitants of the town;
7. Torre de la Catedral: Functioned as a belfry and watchtower, this stone masonry tower was built between 1619 and 1626, facing Plaza Mayor;
8. Casas Reales: The most important architectural complex in the town, it held a prominent position in the public hierarchy. Built on bare rock foundations, its strategic location was the most salubrious, with a dominant position in the town and in relation to the sea. The complex was subjected to constant remodeling after it was seriously damaged during the 1621 earthquake. Following the town's abandonment, the walls endured tidal erosion.

The sampling procedure was performed according to the UNI EN 16085:2012 norm [29], European standard, equivalent to the UNE-EN 16085:2014 already utilized in Latin America [30]. The collection of the specimens was performed in agreement with the indications of the patronage experts, with original material being selected that was not altered by restoration, in order to have the most complete representativeness of all the lithotypes utilized in the masonry. Furthermore, sampling points were chosen on the basis of particular deterioration phenomena, visually detected, in order to evaluate the environmental impact. Finally, possible quarries at the site were also identified and sampled. Specifically, twenty-four samples from the masonry of eight monuments and three samples from outcrops were collected and listed in Table 1.

In order to characterize and evaluate the state of preservation of these materials, the following analyses were performed:

- Stereomicroscope observations were performed by an Optika SZ6745TR, equipped with a webcam, MOTICAM 2005 5.0 Mp,. The Moticam Image Plus 2.0 software was utilized for preliminary analyses of the bulk samples;
- Polarized light microscopy (PLM) was utilized for the observation of the thin sections, using an Olympus BX 51 microscope, equipped with scanner and the MICROMAX software "Primoplus_32" vers. 8.11.02;
- X-ray powder diffraction (XRPD) was used for determining the mineralogical phases present, through a Philips PW 1730 diffractometer equipped with a copper anticathode and a nickel filter. The measurement conditions had a diffraction interval of 2θ, between 5° and 50°, a 2°/minute step at 40 kV voltage, and a 30 mA current intensity. In addition, further analyses were performed in order to verify the clay minerals present in several samples, utilizing a Bruker AXS D8, in Bragg–Brentano geometry, equipped with a X-ray tube and a SolX solid state detector, working in low-temperature through a Peltier cooling system. The samples for this technique underwent the powdering process, utilizing two mills: firstly, a jaw crusher and secondly a mortar grinder with agate jar and pestle. For materials with a high hardness, the process was finished by manual grinding with an agate mortar. Moreover, in order to examine the clay minerals in detail with the second diffractometer, analyses were repeated three times for each sample: the first one on a random mount sample (measurement conditions: time = 2 h 14′; slits = 1, 1, 0.2); then on iso-oriented powder (measurement conditions: time = 1 h 33′; slits = 0.6, 0.6, 0.2; 2θ = 2–30°); and finally, the latter one underwent

ethylene glycol solvation (measurement conditions: time = 1 h 33′; slits = 0.6, 0.6, 0.2; 2θ = 2–30°).

- Environmental scanning electron microscopy and microchemical investigations by energy dispersive X-ray spectrometry (ESEM-EDS) were carried out to determine the elemental composition of specific areas of interest, already observed in the PLM investigation. The instrument utilized was a ZEISS EVO LS 10 with LaB6 source;
- X-ray fluorescence (XRF) on powder pellets (see the XRPD section for the powdering process), using a wavelength-dispersive automated ARL Advant'X spectrometer, was utilized. The accuracy and precision for major elements were estimated to be 2–5%; for trace elements (above 10 ppm), they were above 10%;
- X-ray Fluorescence non-invasive micro-analysis (μXRF) performed using an ARTAX 200 μEDXRF spectrometer equipped by Mo X-ray tube and using a Peltier cooled Si (Li) detector, with a collimator with a diameter from 1 mm, a voltage of 50 kV, and a current of 700 μA (live time: 300 s), on bulk samples in order to evaluate the nature of the chromatic alterations;
- Mercury intrusion porosimetry (MIP) was used for understanding the porosimetry features of the materials and the index of their state of conservation, using a porosimeter "PASCAL 240, THERMO SCIENTIFIC";
- Ion chromatography (IC) was used in order to evaluate the possible presence of soluble salts present in the masonry. IC analyses were performed using a DIONEX ICS 900. Anions analysis: Column S23 Pre-column G23; Cations analysis: Column CS12 Pre-column CG12.

Table 1. Samples, lithotypes (for the definition of breccia see [31]), deterioration patterns [32], location of sampling, pictures and analyses performed. Samples are grouped by structure, while structures are listed from the eastern side to the western side of the site. Legend: SM = stereo microscopy; PLM = polarized light microscopy; ESEM-EDS = environmental scanning electron microscopy and energy dispersive X-ray spectrometry; ts = on thin section; bm = on bulk material; XRPD = X-ray powder diffraction; XRF = X-ray fluorescence; μXRF = X-ray fluorescence non-invasive micro-analysis; MIP = mercury intrusion porosimetry; IC = ion chromatography.

Sample	Lithotype	Deterioration Patterns	Sampling Location	Picture	Analyses Performed
PANAMÁ VIEJO—Masonry					
1. Fortín de la Natividad					
PV FN 1	Breccia	Biological colonization (algae), partial detachment (exfoliation)	S wall—External part, h 100 cm		PLM; XRPD; ESEM-EDS (ts); XRF; IC
PV FN 2	Breccia	No evident deterioration was detected	S wall—External part, h 20 cm		PLM; XRPD; XRF; MIP
PV FN 4	Basaltic andesite	Partial erosion	W wall—Inner part, h 102 cm		PLM; ESEM-EDS (ts); XRPD; XRF; MIP

Table 1. *Cont.*

Sample	Lithotype	Deterioration Patterns	Sampling Location	Picture	Analyses Performed
PV FN 5	Basaltic andesite	No evident deterioration was detected	Inner part of the Fortress, ground level	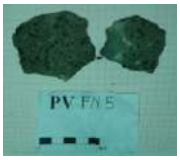	PLM; XRPD; XRF; MIP
2. Convento de San Francisco					
PV FC 4	Breccia	No evident deterioration was detected	E wall of the navy, ground level		PLM; ESEM-EDS (ts); XRPD; XRF; MIP
PV FC 5	Breccia	Exfoliation.	E wall of the navy, h 106 cm		PLM; XRPD; IC
PV FC 6	Rhyodacite	Partial delamination and discoloration	E wall of the Convent, h 170 cm		PLM; ESEM-EDS (ts); XRPD; XRF; MIP; IC
PV FC 7	Breccia	Exfoliation, differential erosion/coving	W wall, h 175 cm		PLM; ESEM-EDS (ts); XRPD; XRF
PV FC 8	Breccia	Exfoliation, differential erosion/alveolization, biological colonization (algae)	W wall, h 100 cm		PLM; XRPD; XRF; IC
PV FC 9	Rhyodacite	Exfoliation, differential erosion/alveolization, partial biological colonization (algae)	W wall, h 200 cm		PLM; XRPD; XRF; IC
PV FC 11	Breccia	Blackening/biological colonization (algae)	S-W side of the wall of the complex 9.70 m from the new via Cinquentenario, h 140 cm		PLM; XRPD; XRF; IC
3. Hospital de San Juan de Dios					
PV SJdD	Rhyodacite	Biological colonization (lichens) and a whitish thin-encrustation on the internal surface	Wall facing the old Via Cinquantenario, h 120–130 cm		PLM; ESEM-EDS (ts); XRPD

Table 1. *Cont.*

Sample	Lithotype	Deterioration Patterns	Sampling Location	Picture	Analyses Performed
4. Convento de las Monjas de la Concepción					
PV CC 4	Breccia	Differential erosion/coving	N side of the chapel, h 140 cm		PLM; XRPD; XRF; MIP
PV CC 5	Breccia	Erosion, biological colonization (algae)	N wall of the nave, h 365 cm		PLM; XRPD; XRF
PV CC 6	Breccia	Differential erosion/coving, biological colonization (algae)	Outer wall of the Church, near an eaves, faced S and exposed to the old Via Cinquantenario, h 165–170 cm		PLM; XRPD; XRF; IC
5. Convento de la Compañia de Jesús					
PV JC 1	Breccia	No evident deterioration was detected (previously covered by plaster, noticed also a bush-hammered surface)	W façade, internal side, inner part of the arch, h 345 cm		PLM; XRPD; XRF; MIP
PV JC 2	Breccia	Biological colonization (algae), probably bush-hammered	W façade, internal side, inner part of the arch, h 300 cm		PLM; XRPD; XRF
PV JC 3	Breccia	No evident deterioration was detected	Near the N façade, ground level		PLM; XRPD; XRF; MIP (2 specimens for MIP analysis have been obtained, thus the results' labels show a and b)
PV JC 4	Breccia	No evident deterioration was detected	W wall, h 293 cm		PLM; XRPD; XRF; MIP; IC
6. Casa Terrin					
PV CT 1	Rhyolite	Biological colonization (lichens) and discoloration (?).	Wall on the W side of Casa Terrin. Sample collected from the N side, h 165 cm		SM; PLM; XRPD; XRF; μXRF; MIP

Table 1. *Cont.*

Sample	Lithotype	Deterioration Patterns	Sampling Location	Picture	Analyses Performed
PV CT 2	Rhyolite	No evident deterioration was detected	Wall on the W side of Casa Terrin. Sample collected near the S-E corner, ground level		PLM; XRPD; XRF; MIP
7. Torre de la Catedral					
PV TC 3	Tuffite	Exfoliation	W wall, h 109 cm		PLM; XRPD; XRF; MIP
PV TC 4	Tuffite	Biological colonization (black algae)	S wall, h 127 cm		SM; PLM; ESEM-EDS (bm); XRPD; XRF; MIP; IC
8. Casas Reales					
PV CR 4	Breccia	Biological colonization (algae), erosion/ delamination	S wall, h 160 cm		PLM; XRPD; XRF; IC
PANAMÁ VIEJO—Outcrops					
PV Q 1	Breccia (volcanoclastic)	Biological colonization (black algae)	Outcrop near Casa Reales		PLM; MIP
PV Q 2	Basaltic andesite	Biological colonization	Quarry near the Santo Domingo Convent		PLM; XRPD; XRF; MIP
PV vic. CR	Basaltic andesite	Biological colonization (black algae)	Outcrop near Casa Reales-Location: Lat. 9°0′20.720″– Long.–79°29′0728″		PLM; XRPD; XRF; MIP

3. Results and Discussion

3.1. Materials Characterization—Outcrops

Three outcrops, i.e., potential quarries, were identified at the site. Specifically, polygenic breccia, mainly composed of volcanic clasts, and basaltic andesite are the lithotypes detected.

In proximity of the Casas Reales complex, near the sea side, two outcrops, one of breccia and one of basaltic andesite, were sampled (Figure 3g). These findings are in agreement with a previous investigation by Grajales Saavedra [28], which identified andesite and agglomerates outcrops in this area. Another outcrop of basaltic andesite was found near

the Convento de Santo Domingo and the Plaza Mayor, in the southern part of the site. This outcrop showed digging traces, as shown in Figure 3h; therefore, it is feasible that it was a quarry.

Polarized light microscopy (PLM) observations showed that the volcanoclastic breccia is mainly characterized by pyroxenes clusters and amygdales filled with secondary minerals due to hydrothermal phases. The basaltic andesites showed the presence of pyroxenes clusters, zoned plagioclases, several amygdales with secondary minerals, and traces of hydrothermal activity.

3.2. Materials Characterization—Masonry

Through the preliminary macroscopic observations of the masonry, sedimentary and volcanic rocks were identified. These findings are in agreement with previous studies that identified these rock types as construction materials [33,34].

Mineralogical and petrographic characterization highlighted that the most diffused lithotype is polygenic breccia, which is present in nearly all of the sampled monuments. The breccia's origin is related to sedimentary processes. In this case, the sediments produced fragments of both volcanogenic and marine origin. Additionally, volcanic rocks, such as basaltic andesite, rhyolite, and tuffite, were found as well.

In more detail, when observing thin sections of polygenic breccias under polarized light microscopy (PLM), clasts deriving from effusive rocks (such as andesites and basalts) and from marine fossils (such as foraminifera, corals, echinoderms, etc.) were detected. In addition, microscopic analysis identified several inner alterations of the volcanogenic fragments. Plagioclases exhibiting zonation and/or sericitization, features associated with hydrothermal alteration, were observed. These alterations derive from the stone formation process [35]. Furthermore, in almost all samples of tuffite and volcanic clasts within breccias, a diffused zeolitization was detected. Lastly, a few samples (PV FC 6, PV FC 9, and PV SJdD), showing a very fine texture and a creamy aspect under the naked eye, were recognized as altered volcanic rocks. Examples of PLM micrographs are shown in Figure 4.

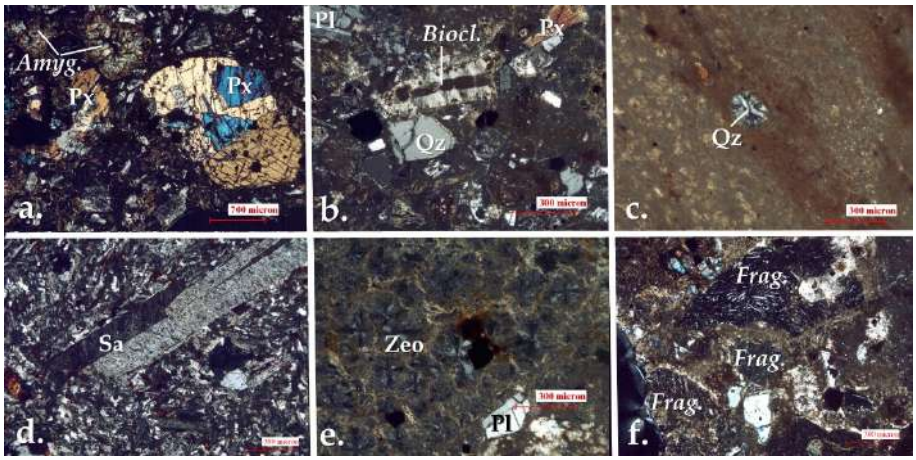

Figure 4. Micrographs of thin sections of samples observed by polarized light microscopy (PLM)-cross-polarized light (xpl): (**a**) PV FN 5 sample: altered pyroxene cluster, amygdale filled with secondary minerals, in a basaltic andesite; (**b**) PV FC 7 sample: foraminifera bioclast, quartz, plagioclase and pyroxenes fragments in a polygenic breccia; (**c**) PV FC 9 sample: a chalcedony filling an amygdale, surrounded by iron oxides in an altered volcanic rock; (**d**) PV CT 2 sample: sanidine and metal oxides in a rhyolite; (**e**) PV TC 4 sample: diffused zeolitization in a tuffite; (**f**) PV CC 4 sample: fragments of basaltic/andesitic lithoclasts in a breccia.

In order to more precisely classify the lava stones, X-ray fluorescence (XRF) analysis was performed, confirming the presence of basaltic andesites, rhyolites, and determining the altered volcanic rocks as rhyodacites (Figures 5 and 6).

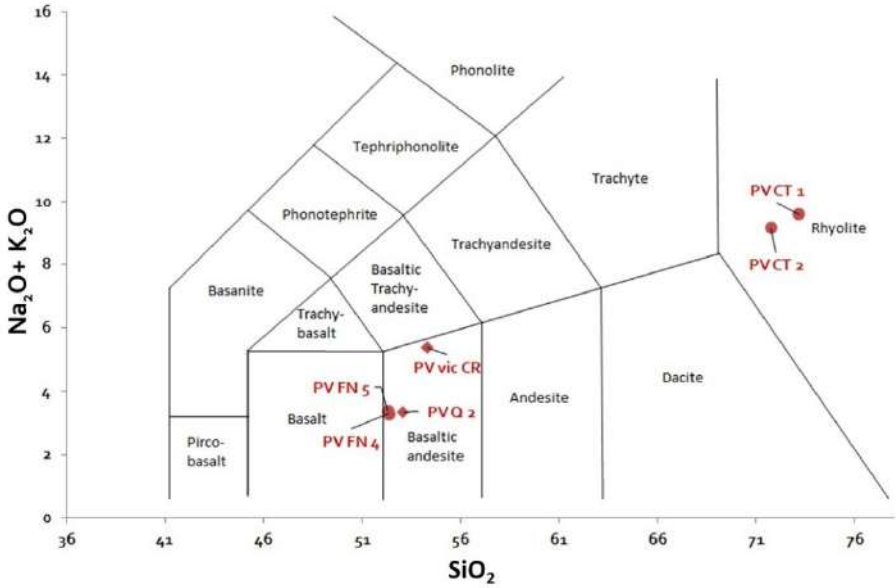

Figure 5. TAS (Total Alkali/Silica) classification [36]. ○ = masonry samples; ◊ = outcrop samples.

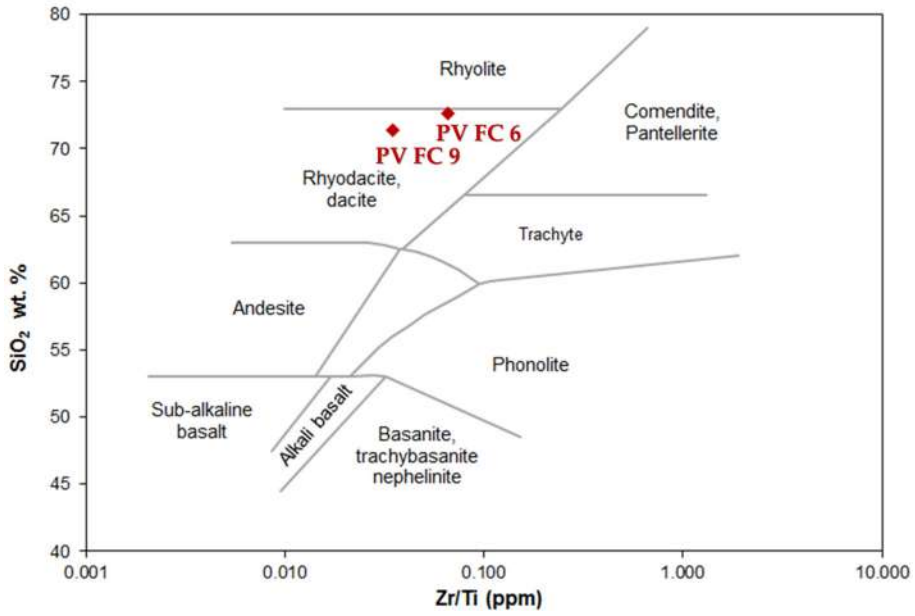

Figure 6. Winchester and Floyd [37] classification for altered volcanic rocks. ◊ = masonry samples.

Specifically, masonry mainly composed of polygenic breccias was identified at the Convento de las Monjas de la Concepción, Convento de la Compañia de Jesús, and Casas Reales. At the Fortín de la Natividad, the stones detected were polygenic breccia and basaltic andesite. Furthermore, at the Convento de San Francisco, both polygenic breccia and rhyodacite were identified. Rhyodacite was also detected at the Hospital de San Juan de Dios. The Torre de la Catedral was predominantly composed of tuffite, while the wall examined at the Casa Terrín complex was entirely constructed from rhyolite.

It was observed that this rhyolite was characterized by sanidine alteration and the presence of iron oxides and/or hydroxides. These formations have a reddish hue, which is often observed to be more concentrated in the external part of the specimens. These alterations were also detected in polygenic breccias and in rhyodacites (e.g., Figure 4c). In sample PV CT 1, a rhyolite fragment, different oxidation in the outer part and the inner part was clearly visible to the naked eye. Non-invasive X-ray fluorescence micro-analysis

showed the different intensity of the Fe peak, highlighting higher external oxidation (Figure 7).

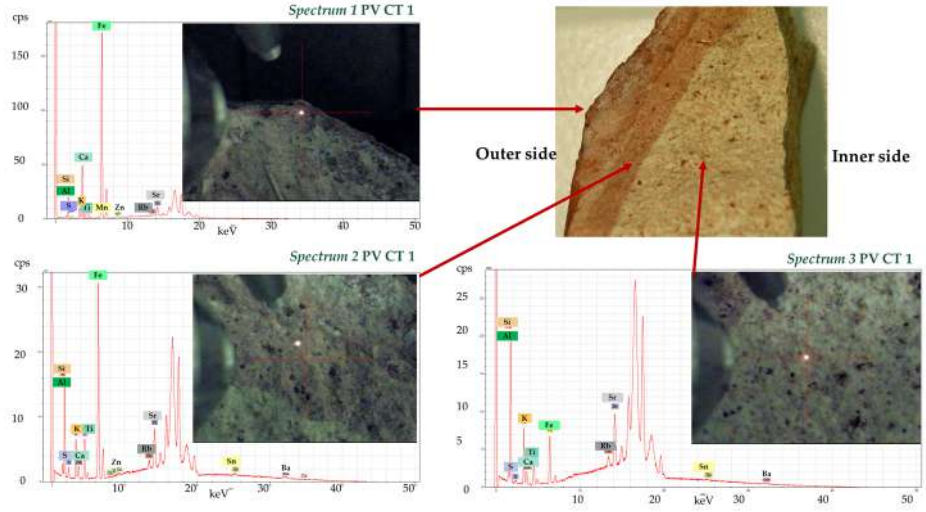

Figure 7. Spectra obtained by X-ray fluorescence non-invasive micro-analysis (μXRF) of the PV CT 1 sample. From the outer side (spectrum 1) to the inner part (spectrum 3).

Contextually, X-ray powder diffraction analysis was performed on almost all samples, with the exception of specimens that exhibited an insufficient amount of material to carry out all the analyses planned. Nevertheless, each rock typology was studied, confirming and/or clarifying the previous investigations and obtaining a complete representation of the mineralogy of the lithotypes under study. In Table 2, the results of the X-ray powder diffraction (XRPD) analysis are summarized, with the crystallographic phases identified in each rock, showing a representative sample per type.

Table 2. Legend: Cal: calcite; Fsp: feldspar; Px: pyroxenes; Qtz: quartz; Zeo: zeolite; Hem: hematite; Kln: kaolinite; Mnt: montmorillonite; Vrm: vermiculite [38]. +++ = dominant; ++ = abundant; + = present, traces; - = absent.

Lithology	e.g., Sample	Cal	Fsp	Px	Qtz	Zeo	Hem	Kln	Mnt	Vrm
Basaltic andesite	PV FN5	-	+++	++	-	-	-	-	tr/+	-
Rhyolite	PV CT1	-	+/++	-	+++	-	tr	tr	-	-
Rhyodacite	PV FC6	-	++	-	+++	+++	-	-	-	-
Polygenic Breccia	PV FC7	+++	++	-	+	++	-	-	-	tr
Tuffite	PV TC4	++	+++	+	++	++	-	-	-	-

Thanks to this investigation, traces of hematite were confirmed within the rhyolite, in addition to traces of kaolinite, a possible symptom of an initial hydrothermal alteration process of the stone and/or weathering during the rock formation [39,40]. Moreover, the aforementioned zeolitization process, observed in breccias and tuffites, was confirmed, detecting clinoptilolite and mordenite. These zeolites were demonstrated to be the main product of alteration caused by hydrothermal processes on vitric tuffs and perlites [41,42]. The rhyodacite samples are characterized by clinoptilolite as the dominant phase (PV FC 9 and PV SJdD) and mordenite (PV FC 6) as the abundant phase, followed by the presence of feldspars.

The finding of clinoptilotite is also in accordance with that of Mumpton [43], who stated that, in Panama, clinoptilolite is one of the most diffused zeolites in rocks originating from volcanic sediments. The presence of zeolites in altered volcanic tuffs is widespread across Latin America. These zeolites give softness to the stone, making them easily workable

and lightweight. These features have made them common construction materials for centuries in Central America [44–46], such as in Mexico, at the Mayan pyramids at Monte Alban and Mitla. Moreover, in this latter example, the pyroclastic sediments show the presence of abundant mordenite and clinoptilolite formed by the alteration of pre-existing glass shards [44], as is also assumable for our samples.

The zeolitized areas underwent scanning electron microscopy and energy dispersive X-ray spectrometry (ESEM-EDS) analysis, performed on thin sections, confirming the previous results obtained by PLM observations and the X-ray powder diffraction (XRPD) analysis. Moreover, in these areas, this investigation identified the possible presence of iron oxides, since the zeolites can exchange ferrous and ferric ions [47], and of silicates of Al, Mg, and Fe attributable to chlorite. In addition, amygdaloidal structures detected in the basaltic andesites were also investigated, revealing that they were mainly filled with radial aggregate of chlorite. This is another mineral that can result from hydrothermal modifications from primary Fe-Mg minerals, such as mica, pyroxene, amphibole, garnet, and olivine. Nevertheless, the formation of chlorite can also be caused by weathering of these mineral precursors [48].

3.3. Evaluation of the State of Conservation

In situ macroscopic analyses allowed us to carry out a first analysis of the deterioration phenomena, summarized in Figure 8.

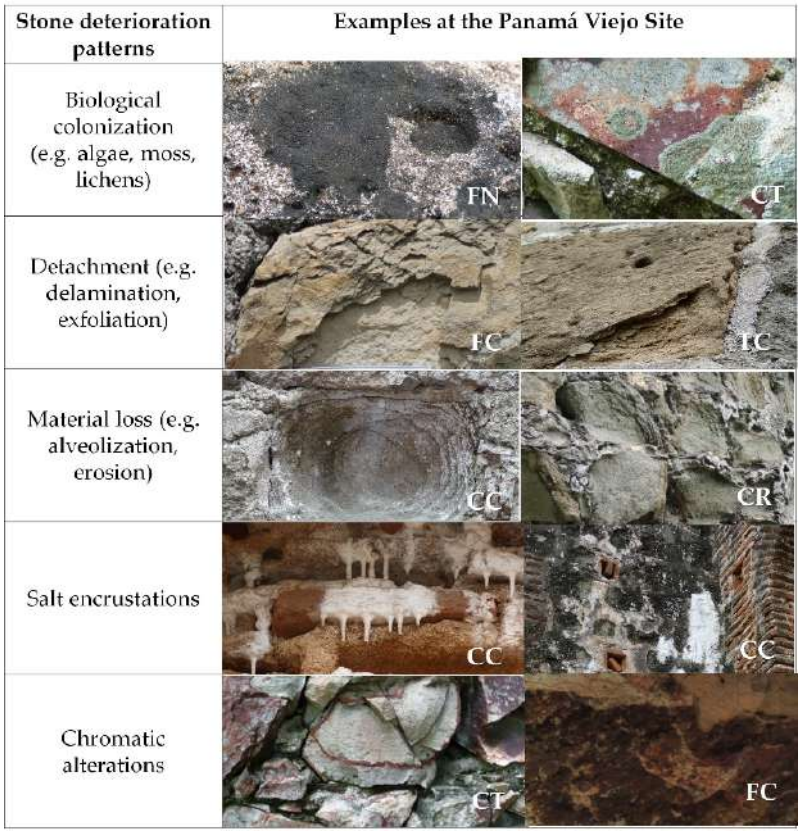

Figure 8. Examples of stone deterioration patterns, according to [32], at the monumental site of Panamá Viejo.

On tuffites and polygenic breccias of the masonries, and in an outcrop of basaltic andesite, black patinas were observed by the naked eye. Then, they were investigated under stereo and scanning electron microscopy, revealing bio-deterioration activity, ascribable to cyanobacteria colonization (Figure 9).

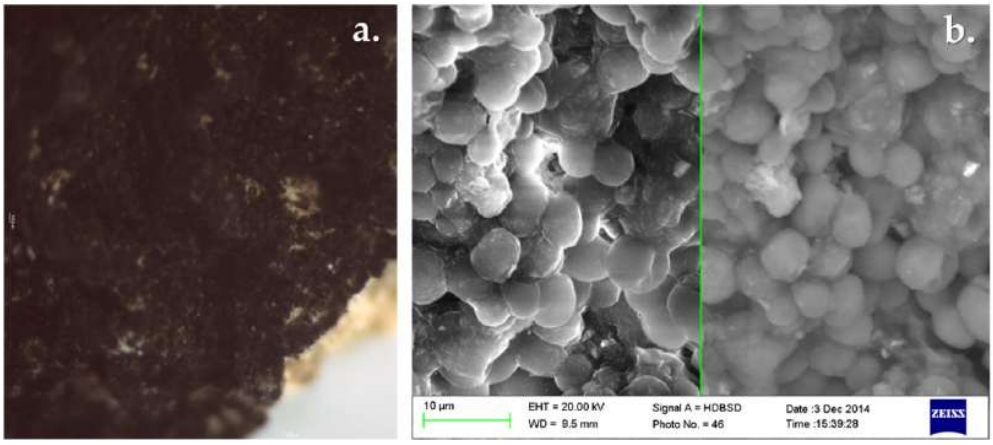

Figure 9. (**a**) Stereo photomicrograph of PV TC 4 sample, showing a superficial black algal patina; (**b**) Scanning electron microscopy (ESEM) photomicrographs (**left**: secondary electrons detector-SE; **right**: backscattered electrons detector-BSD) of PV TC 4 sample, detail of the superficial black algal patina.

The presence of black algae on these monuments was already observed in the work of Torres Montes [33], where "alga negra", a cyanobacteria (*Oscillatoria* sp.) [49], was described. The algal presence is facilitated by the bio-receptivity of the substrate, determined by features such as porosity, surface roughness, and hygroscopicity [50]. These characteristics can also indicate a material prone to wettability. Considering the impact on the stone, the "alga negra" does not represent a direct danger for the material, but it can be a substrate for other bio-deteriogens, and it can trap and retain pollutants. Furthermore, it suggests the presence of high moisture.

On rhyolite and rhyodacite, lichens were observed. These deteriogenic organisms can damage the stone substrate through the production of oxalic acid and other organic acids.

Both macroscopic and microscopic analyses showed the presence of chromatic alteration due to external oxidation, such as iron oxides detected in rhyolites and rhyodacites. These areas represent possible aesthetical damage. Moreover, they could represent a potential point of differential deterioration phenomena, since they show different physical-chemical features in comparison with the core of the rock.

In addition, the presence of clay minerals, in particular montmorillonite and vermiculite, and zeolites can contribute to a significant sensitivity to expansional processes due to the moisture cycles and salt crystallization [51]. Furthermore, microscopic analyses showed that altered parts (such as zeolitized areas) can feature cracks. These aspects can be co-responsible for the observed macroscopic weathering phenomena, such as cracks, flaking, exfoliation, and detachments.

The rhyodacite of the PV SJdD sample, mainly formed by clinoptilotite—$M_{3\text{-}6}(Si_{30}Al_6)O_{72} \cdot 20H_2O$, where M = Ca, K or Na [52]—showed a detached part. Along the internal surface, a whitish patina was identified as well (Figure 10). Under polarized light microscopy (PLM), the aspect was irregular, showing decohesion and a different thickness. The mechanical stress due to the reaction process, responsible for the patina formation, is clearly visible by scanning electron microscopy (ESEM) (Figure 10b). In addition, the microchemical investigation, performed by energy dispersive X-ray spectrometry (EDS), identified Ca as the principal element present in the patina, also with the presence of O, suggesting a composition mainly formed by calcium carbonate (Figure 10c). The development of calcite, as a precipitated secondary mineral, was also supported by its identification in the masonry mortars previously studied [13].

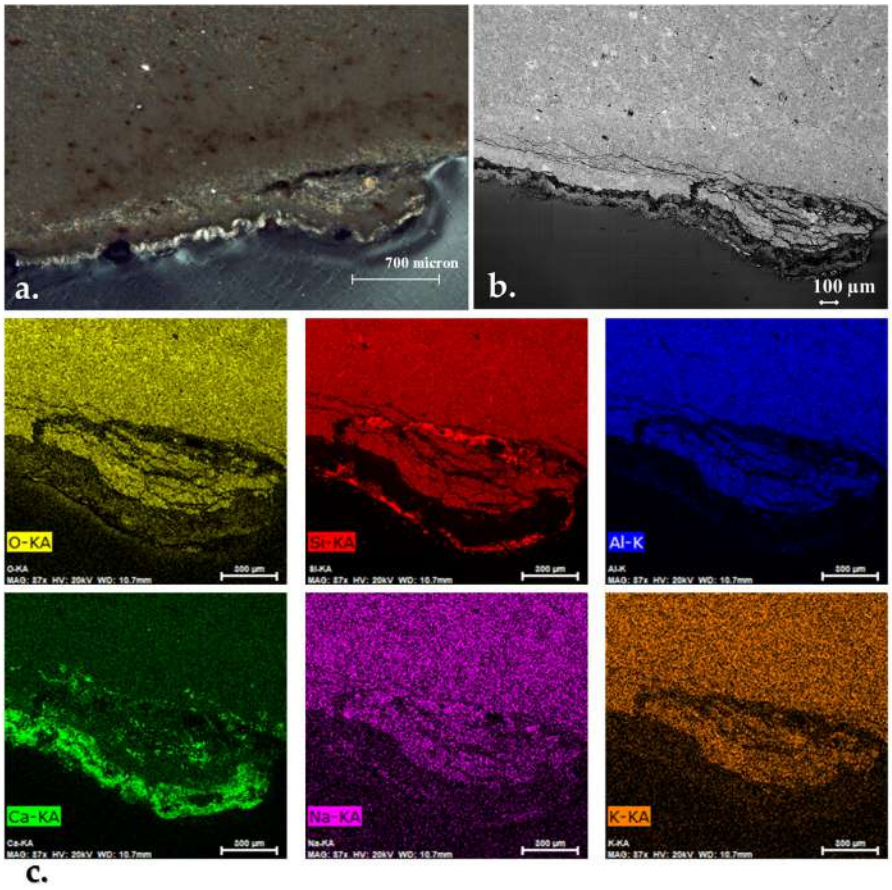

Figure 10. Thin section of the PV SJdD sample showing an altered patina: (**a**) PLM-xpl micrograph; (**b**) ESEM micrograph; (**c**) ESEM-energy dispersive X-ray spectrometry (EDS) microchemical compositional maps.

Analyzing the samples using mercury intrusion porosimetry (MIP), it was noticed that all the samples showed an average pore diameter of less than 0.2 µm, which is the threshold for micropores. Considering the accessible porosity, tuffite and rhyodacite registered the highest values: between 26% and 31%. Polygenic breccia showed variability from approximately 12% to 29.5%; while basaltic andesite and rhyolite had the lowest values, equal to or less than 12%. Detailed results are shown in Table 3.

From a preservation point of view, the porous structure could potentially increase the substrate's bio-receptivity, as previously mentioned. Furthermore, it can undergo possible salt damage, due to the dissolution/crystallization cycles. The salt's solubility and crystallization pressure on the pore walls can be influenced by the size of the pore [53]. The produced stress can cause several forms of damage, depending on where the crystallization occurs. For instance, salt sub-florescence, occurring within the porous stone, can lead to higher decay compared to efflorescence, where the crystallization takes place on the stone's surface [54,55]. The mobility of saline solutions within the material is regulated by several factors. These factors include the structural characteristics of the stone, such as the open porosity, pore size distribution and connectivity, the mechanical and petrographic features, and salt concentration [56].

In order to investigate the possible presence of soluble salts, ion chromatography (IC) analysis was performed on samples showing alteration patinas. The highest values registered belonged to calcium, followed by chloride and sodium, nitrate, sulphate, magnesium, and, rarely, acetate and potassium. Concerning anions, the chloride, nitrate, and sulphate concentration was always <2%, as reported in Table 4, which displays the IC data. The low concentration found explains why salts were not detected by X-ray powder diffraction (XRPD), which has a detection limit of <3–4%.

Table 3. Data of porosity and pore diameter (Ø) of the different samples, gathered in accordance with the same rock typology.

		Accessible Porosity	Inaccessible Porosity	Average Pore Ø	Median Pore Ø	Modal Pore Ø
Lithotype	**Sample**	**%**	**%**	**µm**	**µm**	**µm**
Polygenic breccia	**PV CC 4**	21.21	0.16	0.11	0.60	3.31
	PV FC 4	12.32	0.09	0.06	0.09	0.05
	PV FN 2	25.90	0.05	0.10	0.19	0.14
	PV JC 1	24.09	0.01	0.08	0.15	0.19
	PV JC 3A	27.09	0.02	0.11	0.70	2.44
	PV JC 3B	22.43	0.14	0.06	0.11	0.13
	PV JC 4	15.96	0.33	0.04	0.05	0.06
	PV Q 1	29.52	1.92	0.13	0.38	1.16
Tuffite	**PV TC 3**	30.70	0.25	0.10	0.33	0.82
	PV TC 4	26.50	1.11	0.11	0.27	0.47
Basaltic andesite	**PV FN 4**	10.52	0.16	0.06	0.17	0.04
	PV FN 5	12.14	0.08	0.07	0.22	0.29
	PV Q 2	11.51	0.02	0.05	0.14	0.20
	PV vic. CR	5.23	1.32	0.05	0.08	0.06
Rhyolite	**PV CT 1**	11.57	0.23	0.13	0.20	0.22
	PV CT 2	10.31	0.48	0.10	0.16	0.17
Rhyodacite	**PV FC 6**	27.39	0.15	0.05	0.07	0.06

Table 4. Anion and cation concentrations (ppm) in Panama Viejo samples.

Lithology	Sample	$C_2H_3O_2^-$	PO_4^{3-}	$C_2O_4^=$	CHO_2^-	NO_2^-	NO_3^-	SO_4^-	Cl^-	NH_4^+	K^+	Mg^{2+}	Na^+	Ca^{2+}
Polygenic Breccia	PVFN1	87	0	2	68	11	1183	822	1112	57	325	343	10,076	0
	PVFC5	7	0	319	37	0	258	576	499	25	244	289	2077	2490
	PVFC8	6	42	24	42	0	129	443	565	19	123	199	1178	3038
	PVFC11	14	0	0	53	1	67	173	640	89	354	369	573	19,930
	PVCC6	17	7	0	37	0	115	572	382	0	224	1123	850	27,884
	PVJC4	3	0	0	31	11	3551	2848	3821	0	0	15	287	341
	PVCR 4	6	0	12	25	6	39	162	579	27	314	823	2434	8845
Tuffite	PVTC 4	0	0	34	75	62	6352	3098	10,675	99	237	294	5306	33,039
Rhyodacite	PVFC 6	4	199	0	17	27	1033	775	1739	25	250	288	1518	1787
	PVFC 9	1088	143	0	41	26	1051	634	1334	35	244	353	3672	1775

Considering the Panamanian thermo-hygrometric conditions and the ions detected, possible salt compounds that can crystallize in these circumstances were identified and reported in Table 5, according to the studies of Arnold and Zehnder [23]. For instance, chlorides and nitrates of potassium and sodium, as well as sodium and magnesium sulphates, can be formed under these conditions, since these compounds crystallize easily in humid climates. Considering the potential origin, the presence of halite is feasible due to the proximity with the sea. While sulphates and nitrates can derive from both natural and anthropogenic sources, such as pollution, other building materials and rising damp should also be considered [56,57]. Hydratable salts, such as mirabilite and thernadite, can cause salt weathering caused by the change of volume. Possible pathologies due to their action are decohesion, alveolation, flaking, scaling, and delamination, all phenomena visible in Figure 8 [56].

Table 5. Equilibrium thresholds of RH (%) and T (°C) of some soluble salts that can affect the masonry. Here, we selected the T (°C) range and highlighted the RH values that are most suitable for Panama according to Arnold and Zehnder [23].

	Salt		**Temperature (°C)**		
	Name	**Formula**	**20**	**25**	**30**
Panamanian range	Nitratite	$NaNO_3$	75.4	74.3	73.1
	Halite	NaCl	75.5	75.3	75.1
	Thenardite	Na_2SO_4	82	82.8	84.3
	Sylvite	KCl	85.1	84.3	83.6
	Epsomite	$MgSO_4 \bullet 7H_2O$	90.1	88.3	88
	Natron	$Na_2CO_3 \bullet 10H_2O$	97.9	88.2	83.2
	Mirabilite	$Na_2SO_4 \bullet 10H_2O$	93.6	91.4	87.9
	Niter	KNO_3	94.6	93.6	92.3
	Arcanite	K_2SO_4	97.6	97.3	97

Lastly, in the presence of water, the ions can create an aggressive environment, forming acids, such as hydrochloric, sulfuric, or nitric acid. The chemical action of these compounds can cause the dissolution of carbonate-based stones and mortars [13]. The calcite of secondary precipitation can crystallize within pores (causing internal tensions) and/or on the surface. This can form superficial patinas, such as the one previously observed in Figure 10, and salt encrustations, as shown in Figure 8.

4. Conclusions

The aim of this research work was to thoroughly characterize the stone masonry structures and assess their vulnerability to environmental impact at the UNESCO "Monumental site of Panamá Viejo", located in Panama. For this objective, the identification of the various lithotypes was performed and their state of conservation was analyzed. In addition, potential quarries for the supply of raw materials were identified.

Nowadays, the site hosts buildings constructed during the period between the end of the 16th century and the following century. This study selected eight stonework masonry monuments, which belong to monastic complexes and public and private constructions with a particular and/or strategic function.

Through the analyses performed, stereo, polarized light (PLM) and electronic microscopy (ESEM-EDS), X-ray powder diffraction (XRPD), and X-ray fluorescence (XRF), it was possible to realize a classification of the lithotypes present in the monuments under study. The results revealed that the masonry structures are mainly composed of sedimentary rocks, such as polygenic breccia, formed by fragments of both volcanic and marine origin. Volcanic rocks were also identified, specifically tuffite, rhyodacite, basaltic andesite, and rhyolite. Considering the outcrops, basaltic andesite and breccia, mainly formed by volcanic clasts, were detected.

Concerning the state of conservation, bio-deteriogens were observed, such as black algal patina, potentially a cyanobacteria (*Oscillatoria* sp.). This was mostly diffused on the tuffite and breccia masonry. Furthermore, it was observed on basaltic andesite from an outcrop. On the rhyolite and rhyodacite samples, lichens were detected. Both these organisms potentially represent a source of damage for the stone. Lichens can cause damage through the production of oxalic acid and other organic acids. Considering the black alga, it does not represent a direct danger for the stone, but it can act as a substrate for other bio-deteriogens, and it can trap and retain pollutants. Furthermore, it can be indicative of a high moisture presence and of a material prone to wettability.

The bio-receptivity of the substrate can also be determined by other factors, such as its porosity, studied through mercury intrusion porosimetry (MIP) analysis. Additionally, the porous structure can be affected by salt damage, due to the dissolution/crystallization

cycles. Therefore, ion chromatography (IC) investigations were performed in order to determine the potential soluble salts present in the samples. Considering the results and the Panamanian environmental conditions, the formation of chlorides and nitrates of potassium and sodium is feasible, as the formation of sodium and magnesium sulphates. The salt weathering due to hydratable salts can cause mechanical stress within the structure. This can cause decohesion, alveolation, flaking, scaling, and delamination, all phenomena visible in the studied monuments. In addition, in presence of water, the ions can chemically affect the structure, forming an acid environment. This can cause the dissolution of carbonate-based stones and mortars. In fact, the crystallization of secondary calcite was observed.

A further potential source of mechanical stress is the presence of clay minerals and zeolites, detected by PLM, scanning electron microscopy and energy dispersive X-ray spectrometry (ESEM-EDS) and XRPD investigations. These materials are susceptible to moisture cycles. They can undergo expansional–shrinking processes, contributing to cracks, flaking, exfoliation, and detachments.

Lastly, chromatic alteration was observed. This is due to an oxidation process, such as those related to the iron oxides detected in the outer part of rhyodacite and rhyolite samples. These areas represent aesthetic damage; furthermore, they can undergo differential deterioration phenomena, since they show different physical-chemical features in comparison with the core of the rock.

In conclusion, this work represents a fundamental step for the current and future preservation of this site. Indeed, it represents an instrument for organizing and enhancing the maintenance and restoration works. It allows the operators aimed at preserving the site to know the compositions of the building materials and to understand the problems related with their interaction with the environment. Moreover, it helps limit and prevent the causes of damages, having identified them. In addition, it can be used in the selection of the most suitable and compatible restoration materials, such as consolidants, protective treatments, restoration mortars, etc. Lastly, it will aid in choosing the most similar materials for possible replacements/integrations in the masonries, utilizing the outcrops identified.

Author Contributions: Conceptualization, C.C., A.B., S.I.A.D. and C.V.; methodology, C.C., A.B., S.I.A.D. and C.V.; validation A.B. and C.V.; formal analysis, C.C.; investigation C.C., A.B., S.I.A.D. and C.V.; resources, A.B., C.V. and S.I.A.D.; data curation, C.C.; writing—original draft preparation, C.C.; writing—review and editing, A.B., S.I.A.D., C.V. and C.C.; visualization, C.C.; supervision, A.B., S.I.A.D. and C.V.; project administration, A.B. and S.I.A.D.; funding acquisition, A.B., C.V. and S.I.A.D. All authors have read and agreed to the published version of the manuscript.

Funding: This research received no external funding.

Data Availability Statement: Not applicable.

Acknowledgments: The authors kindly acknowledge all the people of the Patronage of Panama Viejo, of the Institute of Atmospheric Sciences and Climate of the Italian National Research Council (ISAC-CNR) and the Department of Physics and Earth Sciences of the University of Ferrara (Italy) for the support, encouragement, and collaboration for the realization of this study. In particular, for the support in performing the analysis, the authors want to thank Annalisa Martucci, Renzo Tassinari, Sabrina Russo, Salvatore Pepi, Franco Corticelli and Orlando Favoni. Finally, for the sampling collection, a special thank goes to Alessandro Sardella and Giacomo Dondi.

Conflicts of Interest: The authors declare no conflict of interest.

References

1. UNESCO World Heritage Centre. Archaeological Site of Panamá Viejo and Historic District of Panamá. Available online: https://whc.unesco.org/en/list/790/ (accessed on 10 January 2023).
2. Osorio Ugarte, K. Los Atributos Del Valor Universal Excepcional de Una Propiedad Considerada Patrimonio Mundial—El Caso Del Sitio Arqueológico de Panamá Viejo y Distrito Histórico de Panamá. *Canto Rodado Rev. Espec. En Patrim.* **2012**, *7*, 1–28.
3. de Arango, J. El sitio de Panamá Viejo un ejemplo de gestión de patrimonio. *Canto Rodado Rev. Espec. En Patrim.* **2006**, *1*, 1–15.
4. Ciantelli, C. Environmental Impact on UNESCO Heritage Sites in Panama. Ph.D. Thesis, University of Ferrara, Ferrara, Italy, 2017.

5. Arroyo Duarte, S. Conservation, Reuse and Regeneration of Religious Cultural Heritage: The Case of the Archaeological Site of Panama Viejo and the Historic District of Panama. In *Regenerating Cultural Religious Heritage*; Niglio, O., Ed.; Springer Nature: Singapore, 2022; pp. 237–253. ISBN 978-981-19346-9-8.
6. Cubero-Hernández, A.; Raony Silva, E.; Arroyo Duarte, S. Urban Layout of the First Ibero-American Cities on the Continent through Conventual Foundations: The Cases of Santo Domingo (1502) and Panama Viejo (1519). *Land* **2022**, *11*, 2144. [CrossRef]
7. Cubero Hernández, A.; Arroyo Duarte, S. Colonial Architecture in Panama City. Analysis of the Heritage Value of Its Monastic Buildings. *Designs* **2020**, *4*, 57. [CrossRef]
8. Arroyo Duarte, S. Panamá Viejo después de su destrucción. La cartografía, los grabados, las fotografías y las descripciones como ayuda para estudiar la historia del sitio arqueológico de Panamá Viejo. *Canto Rodado Rev. Espec. En Patrim.* **2015**, *10*, 11–38.
9. Embajada de España en Panamá. *Panamá Viejo: De la Aldea a la Urbe = Panamá Viejo: From Village to City*; Araújo, W., Patronato Panamá Viejo, Programa de Patrimonio de la Cooperación Española, Eds.; Embajada de España en Panamá, Patronato Panamá Viejo: Ciudad de Panamá, Panama, 2007; ISBN 978-9962-8811-4-8.
10. Correa de Sanjur, N. *Historia de Panamá año I*; M. Fernández y Cía.: Madrid, Spain, 1986; ISBN 978-84-401-1515-7.
11. Tejeira-Davis, E. *Panamá: Guía de Arquitectura y Paisaje*; Junta de Andalucía: Sevilla, Spain, 2007; ISBN 978-84-8095-518-8.
12. Mena García, C. Panamá En El Siglo XVIII: Trazado Urbano, Materiales y Técnica Constructiva. *Rev. Indias* **1997**, *57*, 369–398. [CrossRef]
13. Ciantelli, C.; Sardella, A.; Arroyo Duarte, S.; Pecchioni, E.; Bonazza, A. The Monumental UNESCO Site of Panamá Viejo: Investigation of the Masonry Mortars. *Heritage* **2022**, *5*, 646–663. [CrossRef]
14. Arroyo Duarte, S. Transformaciones En El Sitio Arqueológico de Panamá Viejo: El Ejemplo de Las Casas Reales. Ph.D. Thesis, Universitat Politècnica de València, Valencia, Spain, 2016.
15. "Carta del fiscal Bartolomé Morquecho", 26 de octubre de 1608, PANAMA, 15: R.9, N. 96, Archivo General de Indias, Sevilla, Spain. Available online: http://pares.mcu.es/ParesBusquedas20/catalogo/description/380615?nm (accessed on 10 June 2023).
16. Roden, G.I. Sea Level Variations at Panama. *J. Geophys. Res.* **1963**, *68*, 5701–5710. [CrossRef]
17. Alba Carranza, M.M. *Geografía Descriptiva de La República de Panamá*, 2nd ed.; El Panamá América: Panama City, Panama, 1946.
18. Jay, D.A. Evolution of Tidal Amplitudes in the Eastern Pacific Ocean. *Geophys. Res. Lett.* **2009**, *36*, L04603. [CrossRef]
19. Strong, N.; Maekawa, T.; Rovira, B. Rates and Patterns of Coastal Erosion for the Panama Viejo Historical and Archeological Site. In Proceedings of the Abstracts with Programs—Geological Society of America, Portland, OR, USA, 18–21 October 2009; Geological Society of America (GSA): Boulder, CO, USA, 2009; Volume 41, p. 156.
20. Arroyo Duarte, S. *Informe Sobre Las Casas Reales Del Sitio Arqueológico de Panamá Viejo*; Patronato Panama Viejo: Panama City, Panama, 2008.
21. Kottek, M.; Grieser, J.; Beck, C.; Rudolf, B.; Rubel, F. World Map of the Köppen-Geiger Climate Classification Updated. *Meteorol. Z.* **2006**, *15*, 259–263. [CrossRef]
22. Ciantelli, C.; Palazzi, E.; von Hardenberg, J.; Vaccaro, C.; Tittarelli, F.; Bonazza, A. How Can Climate Change Affect the UNESCO Cultural Heritage Sites in Panama? *Geosciences* **2018**, *8*, 296. [CrossRef]
23. Arnold, A.; Zehnder, K. Salt Weathering on Monuments. In *Proceedings of the I Simposio Internazionale Bari 7–10 Giugno La Conservazione dei Monumenti Nel Bacino del Mediterraneo*; Fulvio Zezza: Bari, Italy, 1989; pp. 31–58.
24. Autoridad Nacional del Ambiente. *Atlas Ambiental de La República De Panamá*, 1st ed.; Autoridad Nacional del Ambiente: Panama City, Panama, 2010; p. 190. ISBN 978-9962-651-49-9.
25. Camuffo, D. Physical Weathering of Stones. *Sci. Total Environ.* **1995**, *167*, 1–14. [CrossRef]
26. Knutsen, K.L. La Yeguada Volcanic Complex, Western Panama: An Assessment of the Geologic Hazards Using New $^{40}AR/^{39}Ar$ Ages. Master's Thesis, Michigan Technological University, Houghton, MI, USA, 2010.
27. Cunningham, C.G.; Fary, R.W.; Guffanti, M.; Laura, D.; Lee, M.P.; Masters, C.D.; Miller, R.L.; Quinones-Marques, F.; Peebles, R.W.; Reinemund, J.A.; et al. *Earth and Water Resources and Hazards in Central America*; Circular; US Geological Survey: Reston, VA, USA, 1984.
28. Grajales Saavedra, J.A. Aplicación de Los Procesos de Inversión 3D de Pseudo-Secciones de Resistividad Eléctrica Aparente En Los Suelos Del Interior Del Convento de Santo Domingo (Conjunto Monumental Histórico de Panamá Viejo), Estratigrafía de Los Suelos Peri Metrales e Identificación y Patología de Los Materiales y Los Sistemas Estructurales de Sus Ruinas. Graduation. Master's Thesis in Civil Engineering, Universidad Tecnológica de Panamá, Panama City, Panama, 2012.
29. *UNI EN 16085:2012*; Conservation of Cultural Property—Methodology for Sampling from Materials of Cultural Property—General Rules. European Standard: Brussels, Belgium.
30. Lara Calderón, M.L.; Sanz-Arauz, D.; López-Andrés, S.; Pino, I.D. Characterization and Analysis of the Mortars of the Church of Santo Domingo in Quito (Ecuador). *Heritage* **2022**, *5*, 4024–4036. [CrossRef]
31. Saccani, E. *Petrografia Delle Rocce Sedimentarie Terrigene*; Università di Ferrara: Ferrara, Italy, 2014.
32. Vergès-Belmin, V. *ICOMOS-ISCS: Illustrated Glossary on Stone Deterioration Patterns*; Monuments and Sites; English-French Version; ICOMOS: Paris, France, 2008; ISBN 978-2-918086-00-0.
33. Torres Montes, L. *Informe Preliminar Del Examen Mesoscópico de Las Ruinas de Panamá Viejo*; Patronato Panama Viejo: Panama City, Panama, 1996.

34. Sanchez Nava, M. Diagnostico Del Deterioro de Los Materiales Petreos de Construccion de La Ciudad de Panama Viejo, Midiante Su Caracterizacion Fisicoquimica. Bachelor's Thesis, Facultad de Quimica, Universidad Nacional Autonoma de Mexico, Mexico City, Mexico, 2000.
35. Que, M.; Allen, A.R. Sericitization of Plagioclase in the Rosses Granite Complex, Co. Donegal, Ireland. *Mineral. Mag.* **1996**, *60*, 927–936. [CrossRef]
36. Le Maitre, R.W. A Proposal by the IUGS Subcommission on the Systematics of Igneous Rocks for a Chemical Classification of Volcanic Rocks Based on the Total Alkali Silica (TAS) Diagram: (On Behalf of the IUGS Subcommission on the Systematics of Igneous Rocks). *Aust. J. Earth Sci.* **1984**, *31*, 243–255. [CrossRef]
37. Winchester, J.A.; Floyd, P.A. Geochemical Discrimination of Different Magma Series and Their Differentiation Products Using Immobile Elements. *Chem. Geol.* **1977**, *20*, 325–343. [CrossRef]
38. Whitney, D.L.; Evans, B.W. Abbreviations for Names of Rock-Forming Minerals. *Am. Mineral.* **2010**, *95*, 185–187. [CrossRef]
39. Keller, W.D. Hydrothermal Alteration of a Rhyolite Flow Breccia near San Luis Potosi, Mexico, to Refractory Kaolin. *Clays Clay Miner.* **1968**, *16*, 223–229. [CrossRef]
40. Yokoyama, T.; Nakashima, S. Color Development of Iron Oxides during Rhyolite Weathering over 52,000 Years. *Chem. Geol.* **2005**, *219*, 309–320. [CrossRef]
41. Demina, Y.; Frolova, J.; Rychagov, S. Hydrothermal Alterations and Petrophysical Properties: A Case Study of Yagodninskoe Zeolite Deposit, Kamchatka Peninsula. In Proceedings of the World Geothermal Congress, Melbourne, Australia, 19–25 April 2015.
42. Locati, F.; Cravero, F.; Marfil, S.; Lescano, L.; Madsen, L.; Maiza, P. Zeolites in Acid Vitreous Rocks, Southern Mendoza, Argentina. *J. S. Am. Earth Sci.* **2020**, *98*, 102440. [CrossRef]
43. Mumpton, F.A. *Using Zeolites in Agriculture*; Congress of the US, Office of Technology Assessment: Washington, DC, USA, 1985; pp. 144–149.
44. Mumpton, F.A. First Reported Occurrence of Zeolites in Sedimentary Rocks of Mexico. *Am. Mineral.* **1973**, *58*, 287–290.
45. Corzo, M.A. Preface. In *The Unbroken Thread: Conserving the Textile Traditions of Oaxaca*; Kathryn Klein, The Getty Conservation Institute—Los Angeles: Los Angeles, CA, USA, 1997; ISBN 0-89236-380-0.
46. Roque-Malherbe, R. Chapter 12—Applications of Natural Zeolites in Pollution Abatement And Industry. In *Handbook of Surfaces and Interfaces of Materials*; Nalwa, H.S., Ed.; Academic Press: Burlington, MA, USA, 2001; pp. 495–522. ISBN 978-0-12-513910-6.
47. Roque-Malherbe, R.; Diaz-Aguila, C.; Reguera-Ruiz, E.; Fundora-Lliteras, J.; López-Colado, L.; Hernández-Vélez, M. The State of Iron in Natural Zeolites: A Mössbauer Study. *Zeolites* **1990**, *10*, 685–689. [CrossRef]
48. Haldar, S.K. Basic Mineralogy. In *Introduction to Mineralogy and Petrology*; Elsevier: Amsterdam, The Netherlands, 2020; pp. 109–143. ISBN 978-0-12-820585-3.
49. Macedo, M.F.; Miller, A.Z.; Dionísio, A.; Saiz-Jimenez, C. Biodiversity of Cyanobacteria and Green Algae on Monuments in the Mediterranean Basin: An Overview. *Microbiology* **2009**, *155*, 3476–3490. [CrossRef] [PubMed]
50. Caneva, G.; Nugari, M.P.; Salvadori, O. *La Biologia Vegetale per i Beni Culturali*, 2nd ed.; Nardini: Florence, Italy, 2007; ISBN 978-88-404-4153-5.
51. Pötzl, C.; Siegesmund, S.; López-Doncel, R.; Dohrmann, R. Key Parameters of Volcanic Tuffs Used as Building Stone: A Statistical Approach. *Environ. Earth Sci.* **2022**, *81*, 10. [CrossRef]
52. Clinoptilolite. Available online: https://www.mindat.org/min-1082.html (accessed on 13 March 2023).
53. Rijniers, L.A.; Pel, L.; Huinink, H.P.; Kopinga, K. Salt Crystallization as Damage Mechanism in Porous Building Materials—A Nuclear Magnetic Resonance Study. *Magn. Reson. Imaging* **2005**, *23*, 273–276. [CrossRef]
54. Benavente, D. Role of Pore Structure in Salt Crystallisation in Unsaturated Porous Stone. *J. Cryst. Growth* **2004**, *260*, 532–544. [CrossRef]
55. Sena Da Fonseca, B.; Ferreira Pinto, A.P.; Rucha, M.; Alves, M.M.; Montemor, M.F. Damaging Effects of Salt Crystallization on a Porous Limestone after Consolidation Treatments. *Constr. Build. Mater.* **2023**, *374*, 130967. [CrossRef]
56. Lisci, C.; Pires, V.; Sitzia, F.; Mirão, J. Limestones Durability Study on Salt Crystallisation: An Integrated Approach. *Case Stud. Constr. Mater.* **2022**, *17*, e01572. [CrossRef]
57. Sabbioni, C.; Brimblecombe, P.; Cassar, M. *The Atlas of Climate Change Impact on European Cultural Heritage: Scientific Analysis and Management Strategies*; Anthem Press: London, UK, 2010.

Disclaimer/Publisher's Note: The statements, opinions and data contained in all publications are solely those of the individual author(s) and contributor(s) and not of MDPI and/or the editor(s). MDPI and/or the editor(s) disclaim responsibility for any injury to people or property resulting from any ideas, methods, instructions or products referred to in the content.